Journal of the Korean Chemical Society
2017, *Vol. 61, No. 4*
Printed in the Republic of Korea
https://doi.org/10.5012/jkcs.2017.61.4.168

Enhanced Photocatalytic Properties of Visible Light Responsive La/TiO_2–Graphene Composites for the Removal of Rhodamin B in Water

Yonrapach Areerob and Won-Chun Oh*
Department of Advanced Materials Science & Engineering, Hanseo University, Chungnam 356-706, Korea.
**E-mail: wc_oh@hanseo.ac.kr*
(Received March 25, 2017; Accepted May 15, 2017)

ABSTRACT. La/TiO_2 – graphene composites were synthesized in this study, and applied to the photocatalytic degradation of Rhodamine B (RhB) under UV-visible light irradiation. X-ray diffraction (XRD), surface analysis, X-ray photoelectron spectroscopy (XPS) and scanning electron microscopy (SEM), and Transmission electron microscopy (TEM) analysis demonstrated that La/TiO_2 nanoparticles were well distributed on the surface of graphene, and formed the heterostructure of La/TiO_2-graphene. Compared to the pure TiO_2, La/TiO_2-graphene composites displayed much higher photocatalytic activities in RhB degradation under UV-visible light irradiation. The photocatalytic data of La/TiO_2-graphene composites exhibit extended light absorption in the visible light region, and possess better charge separation capability than that of pure TiO_2. The high photocatalytic activity was attributed to the composite's high adsorptivity, extended light absorption, and increased charge separation efficiency, due to the excellent electrical properties of graphene, and the large surface contact between graphene and La/TiO_2 nanoparticles.

Key words: La/TiO_2, Photocatalyst, Rhodamine B, Absorption, Dye degradation

INTRODUCTION

The vigorous and sustained growth of synthetic dye industries is causing the inevitable retraction of the natural dye textile industry. The removal of dyes from textile and dyeing wastewaters before discharge into the environment is of great importance, since even at very low concentration, the presence of dyes is highly visible and toxic to aquatic life, thus damaging the esthetic value of water and reducing the photosynthetic activity of aquatic organisms.[1] Textile dyes, including Rhodamine B, Methylene Blue and Texbrite, are used in the food, cosmetic and pharmaceutical industries, and represent 90% of consumed food dyes in the United Sates.[2] These dyes can reach the environment through the discharge of industrial and domestic effluents. For example, in the textile industry, 10–15% of dyes are released to the aquatic environment during the dyeing process, and in the case of direct and reactive dyes, almost 30% can be found in the final effluent.[3]

In the past few decades, the advanced oxidation technology of semiconductor titanium dioxide photocatalysis has attracted much attention, owing to its wide application to complete mineralization of various organic pollutants in wastewater and air. Due to its attractive properties, such as good chemical stability, non-toxicity, low cost, and high photocatalytic efficiency[4–6] TiO_2 remains the most promising material for photocatalysts, gas sensors, solar cells, and white pigment. However, the photocatalytic efficiency at present is still very low, which is mainly caused by the fast recombination of photogenerated electron–hole pairs during photocatalysis. Therefore, the doping of metal or nonmetal ions is a useful technique for enhancing the photocatalytic activity of TiO_2.[7] Metal doping induces localized states between the valence band and the conduction band. These mid-gap states could temporarily trap the photogenerated electron–hole pairs,[8] and thus suppress the recombination of charge carriers. Some recent research has focused on the doping of TiO_2 by lanthanide ions with 4f electron configuration. Lanthanide ions can form complexes with various Lewis bases, including organic acids, amines, aldehydes, alcohols, and thiols, by the interaction of the functional groups with their f-orbital. Thus, doping lanthanide ions into a TiO_2 matrix could provide a means to concentrate organic pollutants on the semiconductor surface, and can therefore improve the separation efficiency of photo-induced electron–hole pairs of TiO_2 to enhance the photo reactivity.

The photocatalytic properties of TiO_2 are derived from the formation of photogenerated charge carriers, which process occurs upon the absorption of ultraviolet light corresponding to the band gap. However, TiO_2, with its large band gap (~3.2 eV),[9–11] has a limited adsorption of solar light and low photocatalytic activity, due to the fast recombination of charge carriers. In general, the band structure can be adjusted to enhance its photocatalytic activity by improving its

visible light response and charge separation. The combination of TiO_2 with graphene has received great interest for graphene acting as an acceptor for the photogenerated electrons.

Graphene, a monolayered hexagonal sp^2 hybridized carbon flat, has attracted much attention due to its promising applications in the fields of flexible electronics, photovoltaics, and sensing, as well as photocatalysis.[12] GO has emerged as a precursor offering the potential of cost-effective, large-scale production of graphene-based materials. The good optical transmittance, large specific surface area,[13] and high intrinsic electron mobility make it an ideal material to couple with TiO_2 for photocatalytic reactions.[14] Various TiO_2-graphene composites have been developed and applied in environmental remediation,[15–17] water splitting, CO_2 photo reduction,[18,19] etc. Most research has focused on the loading of TiO_2 nanoparticles onto graphene sheets or other graphene materials. However, TiO_2-graphene composites with porous structure are rarely reported. The composites with porous structure have large surface area and good permeability, which can increase the active sites and light utilization by multiscattering of incidence light, which makes them ideal candidates for high-efficiency photocatalysts.[20–22]

In this study, a two-step hydrothermal process was adopted to prepare La/TiO_2 graphene composites. The influence of lanthanum doping on TiO_2-graphene composites was investigated by degradation of RhB or methylene blue under visible-light irradiation. The prepared La/TiO_2-graphene composites exhibited extended visible-light absorption and greater adsorptivity of RhB enhanced photocatalytic activity than pure TiO_2. In addition, the effect of pH, catalyst dosage and initial dye concentration were determined, and the possible mechanism for the enhanced performance of La/TiO_2-graphene was also proposed.

EXPERIMENTAL

Preparation of Graphene-La/TiO_2 Composites

In the first step, the lanthanum doped TiO_2 samples were synthesized by a hydrothermal method. During this process, 15 ml of tetrabutyl titanate was dissolved in 80 ml ethanol, and 40 ml of distilled water at pH 3.0 (6M HCl) was added to this solution dropwise under vigorous stirring. A given amount of $La(NO_3)_3 \cdot 6H_2O$ was then added to the above solution, and it was stirred for 1 h. After this, the resulting suspension was put into 200 ml Teflon- sealed autoclave, and maintained at 180 °C for 6 h. Finally, the suspension was washed with deionized water, and centrifuged several times to get pH 7. Then samples were dried at 100 °C in the vacuum oven for 12 h, and calcined at 450 °C to obtain La-doped TiO_2 nanopowder. The atomic ratios of La/TiO_2 were 0.5%, 1.0%, and 1.5%.

Graphene oxide (GO) from graphite powder (99.99% Alfa Aesar) was synthesized according to our previous report.[23] In the second step, La/TiO_2-graphene composites were obtained by a hydrothermal method. Briefly, 20 mg of graphene oxide was dissolved in a solution of distilled water (80 ml) and ethanol (40 ml), followed by 3 h ultrasonic treatment; and then 200 mg of TiO_2 or La/TiO_2 with different atomic ratio of La was added, and stirred for 2 h to get a homogeneous suspension. The suspension was then put into a 200 ml Teflon-sealed autoclave, and maintained at 120 °C for 3 h, to simultaneously achieve the reduction of graphene oxide, and the deposition of TiO_2 on the graphene sheets. Finally, the resulting composite obtained by the above procedure was recovered by filtration, rinsed by deionized water ten times, and dried at 70 °C for 12 h.

Characterization

The crystal structure of samples was characterized by powder X-ray diffraction (XRD) by Rigaku D/max-3B X-ray diffractometry with Cu K as radiation source (= 0.15406 nm) at 40 kV and 36 mA. The morphology was observed by JEOL JEM-1200EX electron microscopy operating at 200 kV. The samples for TEM were prepared by dispersing the final powder in ethanol, and the dispersion was then dropped onto carbon–copper grids. The chemical composition of samples was analyzed by X-ray photoelectron spectroscopy (Thermo-VG Scientific, ESCALAB250, monochromatic Al KX-ray source). The binding energy of XPS spectra was calibrated with reference to the C 1s peak (284.6 eV) arising from adventitious carbon. The UV–vis absorption spectra were measured under the diffuse reflectance mode in the range of 300–800 nm by HITACHI U-4100 UV–vis spectrometry with an integrating sphere accessory.

Measurement of Photocatalytic Activity

A self-assembled apparatus with a metal halogen lamp (HQIBT, 400 W/D, OSRAM, Germany) as the radiation source was used to estimate the photocatalytic activity of different samples by monitoring the degradation of RhB. The visible-light (≥ 555 nm) used in the present study was obtained by a filter with the cut-off wavelength of 555 nm. In each experiment, 0.1 g photocatalyst was suspended in 100 ml RhB solution with a concentration of 10 mg L^{-1} in a beaker. Prior to irradiation, the mixed liquor was magnetically stirred for 1 h, to reach the adsorption/desorption equilibration. Following this, the photocatalytic reaction

was started by the exposure of visible light, and the temperature of the suspension was kept at about 20 °C by an external cooling jacket with recycled water. At irradiation time of every 0.5 h, 5 ml suspension was sampled, centrifuged, and the supernatant was taken out for UV–vis absorption measurement. The intensity of the main absorption peak (555 nm) of the RhB dye was referred to as a measure of the residual dye concentration (C).

RESULTS AND DISCUSSION

Characterization

Fig. 1 shows XRD patterns of TiO_2 and La/TiO_2-graphene composites with different amounts of La doping. XRD analysis reveals that TiO_2 and composite photocatalysis were comprised of anatase phase structure of TiO_2, namely, the planes (101), (004), (200), (211), (204), (220), and (215) at 2ø values of ca. 25.3, 38.0, 48.0, 54.1, 62.6, 69.6, and 75.2°, respectively, which all are in good agreement with JCPDS-21-1272. No intense diffraction peaks related to the oxides of La were observed. It can be seen that after lanthanum doping, the main diffraction peak (101) at 25.3° of anatase TiO_2 was not shifted to higher or lower angle. The ionic radius of La^{3+} is 0.115 nm, which is much larger than that of Ti^{4+} (0.064 nm), so distortion of the lattice will occur only if La^{3+} replaces Ti^{4+} in TiO_2 lattice.[24] The diffraction peaks of lanthanum modified TiO_2 nanopowders are nearly the same as that of pure TiO_2, which indicates that La^{3+} ions may be present in the form of La_2O_3. *Fig.* 1 compares the enlarged anatase (101) peaks for pure TiO_2 and TiO_2-graphene samples. An additional diffraction shoulder peak partially overlapping anatase (101) peak was observed

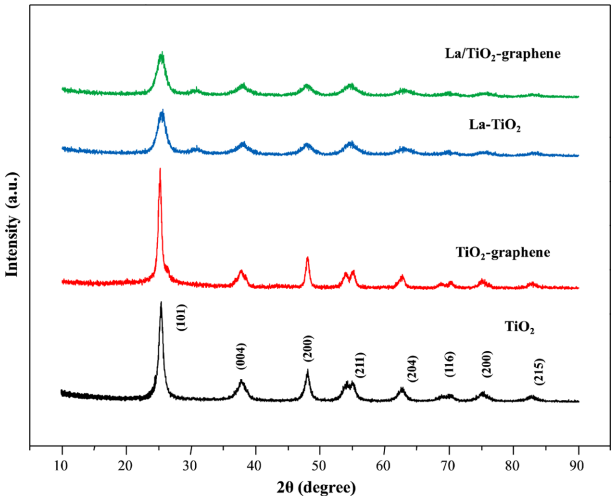

***Figure* 1.** XRD patterns of TiO_2, TiO_2-graphene, La/TiO_2 and La/TiO_2-graphene nanoparticles.

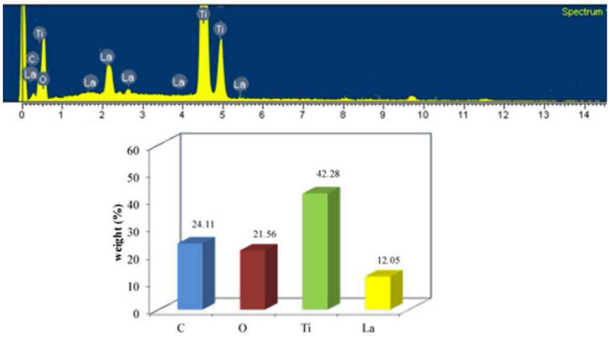

***Figure* 2.** EDX spectrum of the La/TiO_2-graphene nanocomposite for La, C, O, Ti elements and percentage of elements in La/TiO_2-graphene nanoparticles.

in the composite sample, which shows the presence of graphene.[25] In addition, the average crystallite size was determined from the Scherrer's equation using the diffraction peaks at 25.3° and the average nanocrystallite sizes were found to be about 10 nm for La-doped. The decrease in the crystal size can be attributed to the presence of La_2O_3 formed on the surface and on the interstitial sites of the samples, which inhibits the agglomeration of the TiO_2 nanoparticles and inhibit the growth of crystal grains. Further confirmation of the involvement of La/TiO_2-graphene was done by energy dispersive X-ray (EDX) analysis. The spectrum shows strong peaks of La, and the presence of C, O, and Ti in the sample. *Fig.* 2(a) and (b) show that the graphene was successfully combined with La/TiO_2. The weight percentages of C, O, La and Ti in the prepared La/TiO_2-graphene nanocomposite were 24.11, 21.56, 46.76, 12.05 and 42.28%, respectively.

Fig. 3 shows the morphology of synthesized photcatalysts under SEM microscopy. Pure TiO_2 and La/TiO_2 samples (*Fig.* 3(a) and (b)) show that the particles are well separated, devoid of aggregation, and in the size range of 8–12 nm. There is a uniform surface morphology without any cracks in micro-structure among different mass of $La(NO_3)_3 \cdot 6H_2O$ doped TiO_2. Moreover, different quantity $La(NO_3)_3 \cdot 6H_2O$ doped TiO_2 shows more irregular mesopores than pure TiO_2, which contribute to the increase of surface area to the benefit of dye adsorption. *Fig.* 3(c) and (d) show SEM imagery of TiO_2-graphene and La/TiO_2-graphene composite; the obtained composite retained the two-dimensional sheet structure after the hydrothermal process. Because of the distribution of functional groups of graphene oxide, the TiO_2 nanoparticles dispersed on the graphene sheet showed a tendency to accumulate along the wrinkles and edges. In addition, the surface morphology of pure graphene, TiO_2-graphene and La/TiO_2-graphene compos-

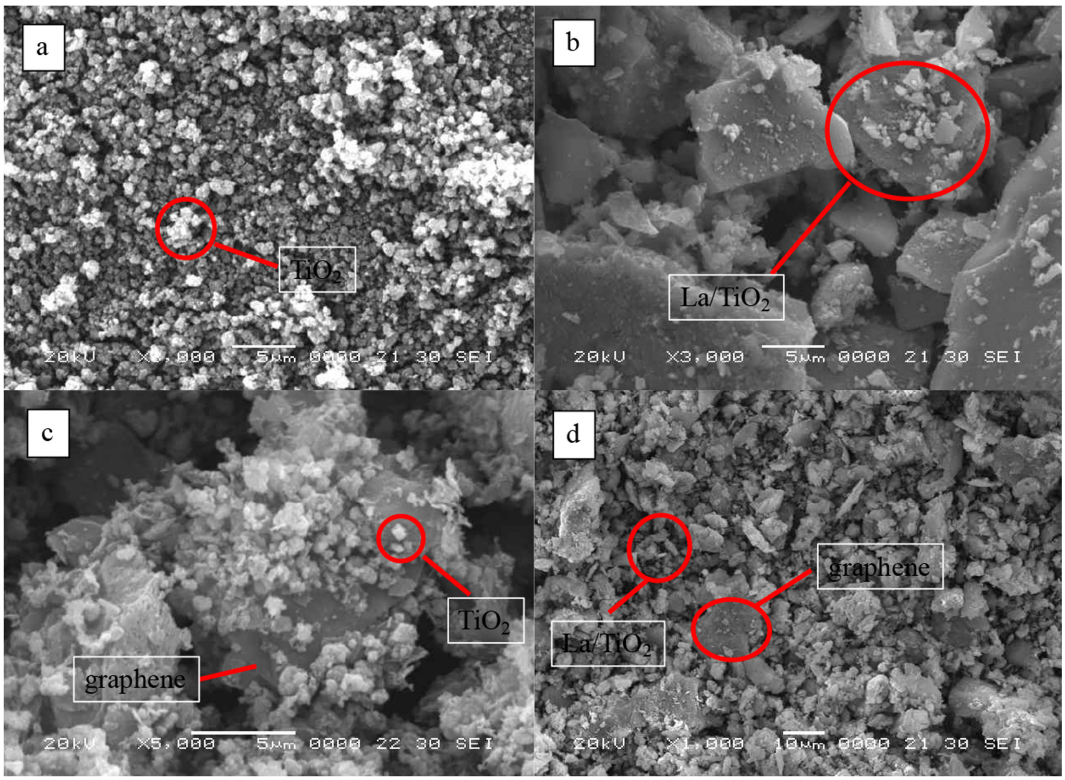

***Figure* 3.** SEM images of (a) TiO_2, (b) La/TiO_2, (c) TiO_2-graphene, and (d) La/TiO_2-graphene composite.

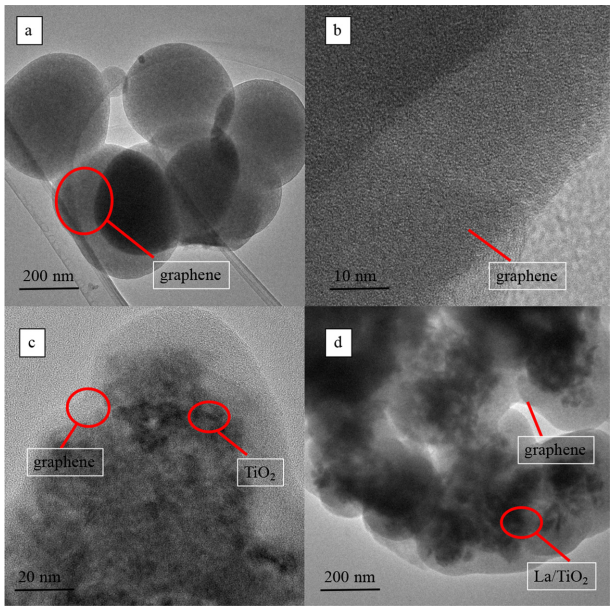

***Figure* 4.** TEM images of TiO_2 with (a) lower magnification and (b) higher magnification, (c) TiO_2-graphene, and (d) La/TiO_2-graphene composite.

ite photocatalysts were characterized by TEM, and *Fig.* 4 shows the imagery. *Fig.* 4(a) and (b) demonstrate the GR layers, while *Fig.* 4(c) shows TEM imagery of the TiO_2-graphene that results in bounding between the anatase nanocrystals of TiO_2 with wide distribution on very thin and transparent graphene sheet, and also shows a ~1 μm wide graphene sheet entrapping a bundle of TiO_2 nanoparticles. Moreover, it is evident that La/TiO_2 nanoparticles were densely embedded into the thin layer of graphene sheets (*Fig.* 4(d)). Therefore, good contact and interaction between La/TiO_2 nanoparticles and graphene achieved by the hydrothermal process is believed to be favorable to transferring the photogenerated electrons into a La/TiO_2-graphene composite system during photocatalysis.

Raman spectroscopy is a highly sensitive characterization technique to obtain the structural information of carbon-based materials.[26] *Fig.* 5 shows the Raman spectrum of synthesized GO that was recorded in the spectral range of 400–2,400 cm^{-1}. Raman spectroscopy of carbon-based materials is usually characterized by considering two main features: the graphitic peak (G), and the diamond peak (D). The G peak arises from the first order scattering of the optical E_{2g} phonon of the sp^2 carbon atoms at the Brillouin zone center (generally observed at 1,575 cm^{-1}), while the D peak (1,345 cm^{-1}), comes from the breathing mode of k-point photons with A_{1g} symmetry. The D peak is Raman active only in the presence of defects. The intensity of the D peak is often used to measure the degree of lattice dis-

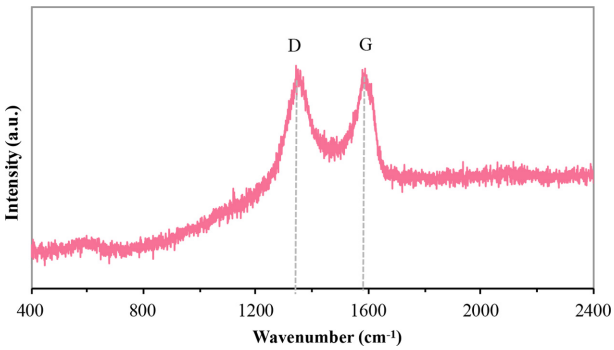

***Figure* 5.** Raman spectrum of graphene.

tortion.[27,28] In the present study, the G and D peaks of GO appear at 1,599 and 1,369 cm^{-1}, respectively. The appearance of G and D peaks in higher wavenumber regions indicates the formation of defects caused by the destruction of the sp^2 network of carbon atoms due to the oxidation process. During the oxidation process, the oxygen-containing functional groups are attached to the basal planes and edges of GO, which creates defects in the structure of GO. In addition, the higher intensity of D peak than G peak, along with their large full-width at half-maximum (FWHM), also indicates considerable structural disorder in GO. The relative intensity of the D band to the G band (ID/IG) is calculated to be about 1.14. The higher intensity value of ID/IG ratio confirms the higher disorder density.

The chemical structure of synthesized GO is identified by FT-IR spectroscopy. *Fig.* 6 shows the FT-IR spectrum of as synthesized GO. The spectrum was recorded in the spectral range of 4,000–400 cm^{-1}. The FT-IR spectrum also makes possible to investigate the presence of oxygen-containing functional groups formed by the oxidation process.

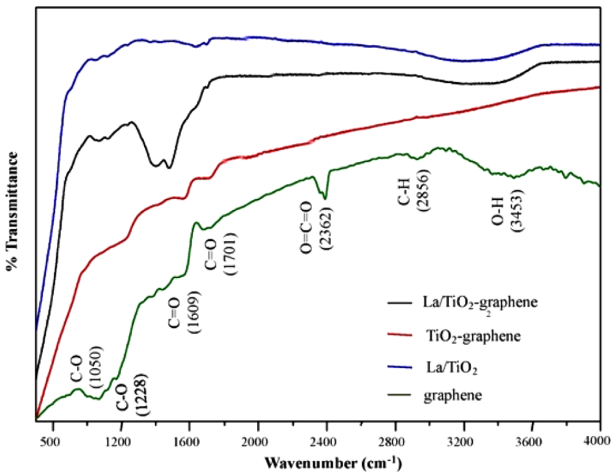

***Figure* 6.** FT-IR spectrum of graphene, TiO_2-graphene, La/TiO_2, and La/TiO_2-graphene.

Fig. 5 demonstrates the presence of several oxygen-containing functional groups, such as hydroxyl (3,453 cm^{-1}), epoxy (1,228 cm^{-1}), carbonyl (1,701 cm^{-1}), and ether (586 cm^{-1}) groups, indicating a high degree of oxidation of the synthesized GO.[29] These oxygen-containing functional groups are attached to the basal planes and edges of GO sheets.[30] The characteristic peaks of GO are detected at 3,436 and 1,050 cm^{-1}, due to O-H and C-O stretching vibrations, respectively[31]. The peak appearing at 1,228 cm^{-1} is due to C-O stretching in the epoxy group, while that at 1,701 cm^{-1} is due to C=O stretching vibration in the carboxylic acid group. The peak corresponding to 1,609 cm^{-1} is due to C=C stretching vibration from unoxidized sp^2 C-C bonds.[32] FT-IR results of the present study are consistent with previous reports. The presence of polar oxygen-containing functional groups strongly changes the van der Waals interactions between GO layers, and makes it hydrophilic. Due to the hydrophilic nature, GO can easily be dispersed in water, and forms a stable colloidal aqueous suspension.

To investigate the chemical states of dopant in TiO_2, XPS survey and core levels spectra of Ti 2p, O 1s, C 1s and La 3d were measured. *Fig.* 7a shows the XPS survey spectrum of graphene-La/TiO_2 composite, which contains 0.6% La 3d, 54% O 1s, 26% Ti 2p, and 19.4% C 1s. The core level XPS spectrum of Ti 2p shows that the Ti 2p region is composed of Ti 2p 3/2 and Ti 2p 1/2 peaks. The

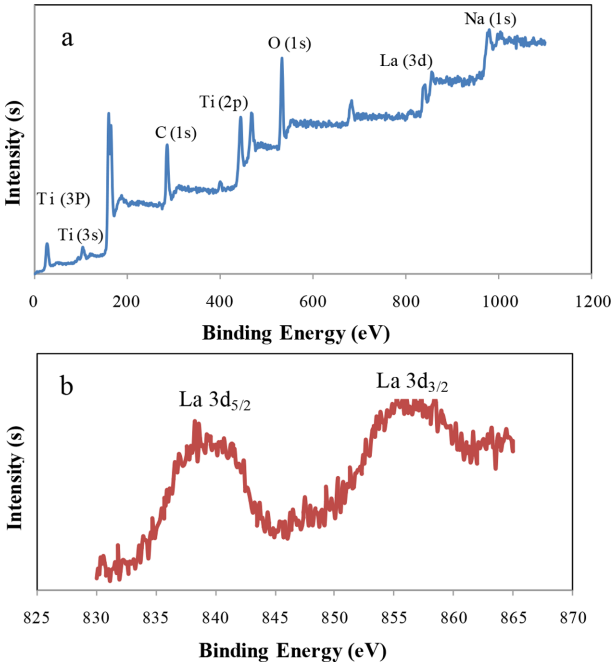

***Figure* 7.** XPS spectrum for (a) La/TiO_2-graphene and (b) of the core levels of La 3d band.

binding energies of these peaks are 459.3 and 465.1 eV, respectively, which agree well with the data reported by other researchers.[33,34] This also indicates that all Ti in powders exist in the form of TiO_2. O 1s core level spectrum shows a main peak at 530.1 eV, which can be ascribed to the metallic oxides (Ti=O bonds), which is consistent with the binding energy of O^{2-} in the TiO_2 lattice; and another peak at 530.9 eV is for oxygen atoms in the surface hydroxyl groups (H-O bonds) and/or in the carboxyl groups (C=O bonds).[35] Regarding the La 3d core level spectrum (*Fig.* 7b), we observed the splitting of the La $3d_{5/2}$, La $3d_{3/2}$ at around 835.4 eV and 852.2 eV respectively. Combined with the XRD results, the La 3d XPS profile observed in our sample is most probably as a form of lanthanum oxide (La_2O_3).

Fig. 8 and *Table* 1 show the BET surface area, pore volume, peak pore size, and average pore diameter of La/TiO_2-graphene. Since the photocatalytic performance of the materials is highly dependent on their amount of surface, surface area measurements were performed by the BET method. The samples were analyzed by subjecting them to BJH cumulative adsorption volume of pores with diameter between 3.77 nm is 0.06 cm^3/g for La/TiO_2-graphene. It is apparent that the higher specific surface area, along with the increase of La content, was the essential factor to adsorb more dye. Thus, La/TiO_2-graphene composites may be an excellent candidate for adsorption and photocatalyst.[35,36]

Photocatalytic Activity

The photocatalytic activity is significantly dependent on the adsorption capability and transportation of electron–hole pairs. To investigate the adsorption capability of the prepared samples, the adsorption experiment was carried out for RhB for 1 h using 10 mg amount of different catalysts at room temperature under the dark. *Fig.* 9 shows the typical absorption peaks at 555 nm for RhB absorption change decrease after 10 min, which confirms the complete removal of RhB by the La/TiO_2-graphene composite photocatalyst. At the same time, a spectral blue-shift from 501

***Table* 1.** Physical properties of different material nanomaterials

Catalyst	Surface area (m^2/g)	Pore volume (cm^3/g)	Pore size (Å)
TiO_2	12.66	0.1593	65.5
La/TiO_2	63.74	0.1617	45.1
La/TiO_2-graphene	73.23	0.1634	26.7

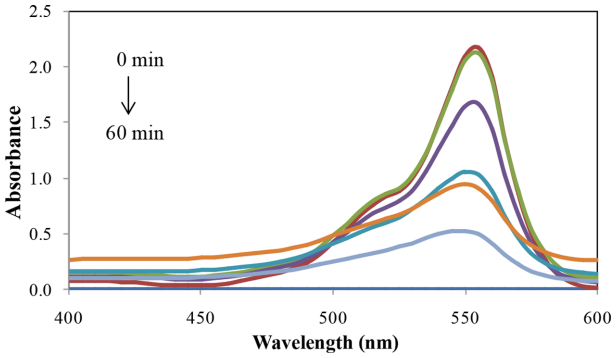

***Figure* 9.** Absorption changes of RhB with different adsorption periods. Experimental condition: [nanocatalyst]=10 mg; [dye]=25 mg/L; [temperature]=25 °C; [reaction time]=0-60 min.

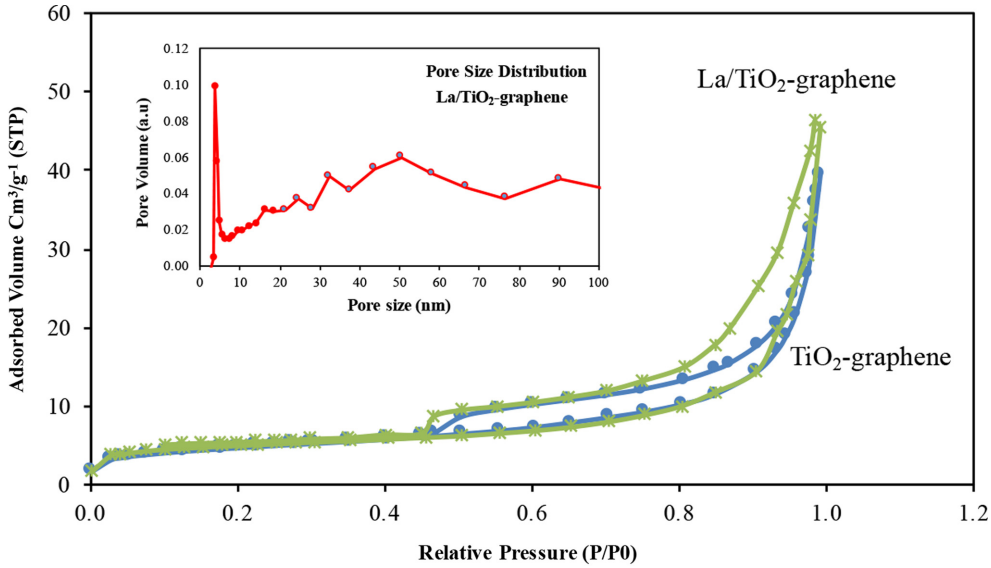

***Figure* 8.** N_2 adsorption-desorption isotherms at 77 K for La/TiO_2-graphene and inset representing pore size distribution of La/TiO_2-graphene.

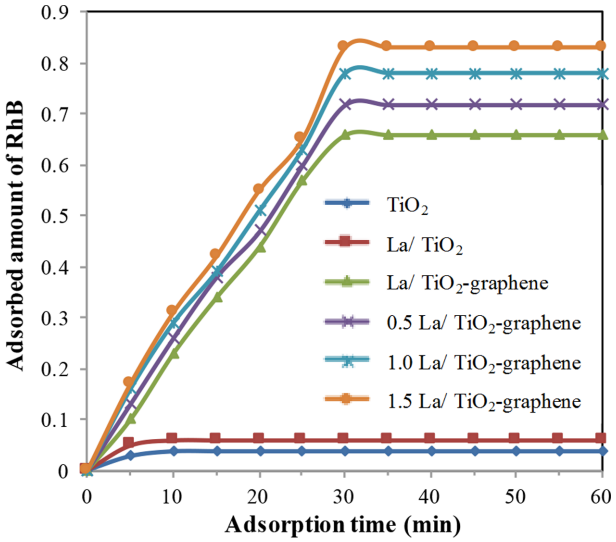

***Figure* 10.** Absorption efficiency of RhB on TiO_2, La/TiO_2, La/TiO_2-graphene, 0.5 La/TiO_2-graphene, 1.0 La/TiO_2-graphene, and 1.5 La/TiO_2-graphene. Experimental condition: [nanocatalyst]=10 mg of different catalysts; [temperature]=25 °C; [reaction time]= 0-60 min under the dark.

to 555 nm can be noted in *Fig*. 9, which can be ascribed to the de-ethylation processes in the RhB dye photodegradation. In addition (*Fig*. 10), the results indicate that under the present conditions, adsorption equilibrium can be reached within 30 min for all samples. The 1.5 La/TiO_2-graphene composite sample has superior adsorption capability for RhB to the other samples, due to the giant-conjugation system and two-dimensional planar structure of graphene and appropriate amount of La in the composite sample. Moreover, the enhanced adsorption of RhB was driven by the stacking between RhB and aromatic regions of graphene.[37,38]

The photocatalytic activities of different La doped (0.5, 1.0 and 1.5%) TiO_2-graphene, and also La doped TiO_2 samples, were evaluated by photodegradation of RhB as model reaction under visible-light irradiation. *Fig*. 11 presents the results of the photocatalytic activity of different samples. Three factors play a crucial role in photocatalysis, including the light absorption, adsorption of organic contaminant molecules and the separation of excited electron-hole pairs. Therefore, we can observe that TiO_2showed rather poor photocatalytic activity compared with other samples upon irradiation under visible light irradiation. The degradation rate under visible-light irradiation increased directly with the increase of the amounts of La doping level up to 1.5%. Further increase of the amount of La doping decreased the photocatalytic activity of the catalyst, indicating the presence of an optimal loading. The decrease in the activity with higher La ratio in the composite sample is considered to

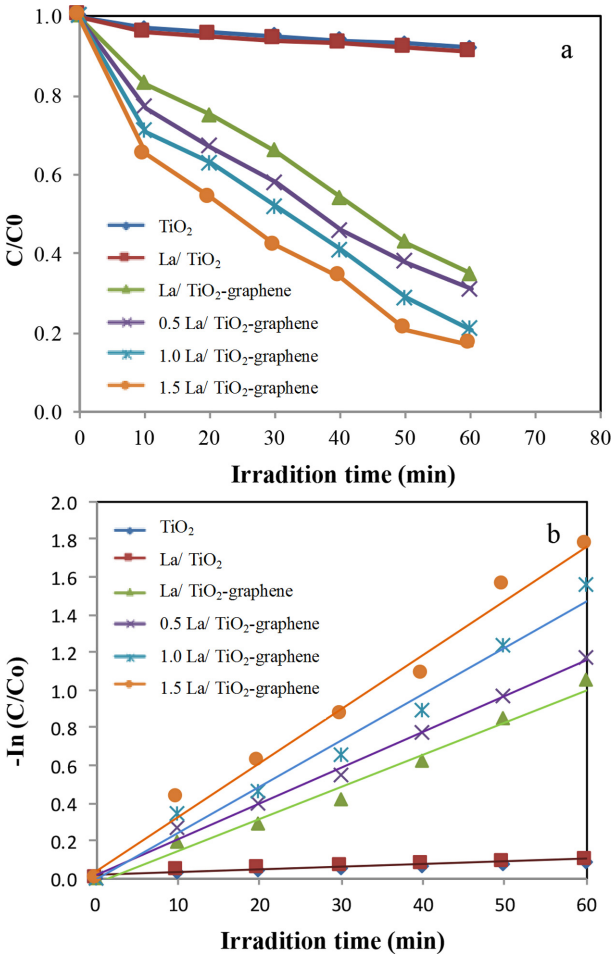

***Figure* 11.** The photodegradation of RhB in form of (a) C/C0 and (b) -ln(C/C0) under visible light irradiation over the TiO_2, La/TiO_2, La/TiO_2-graphene, 0.5 La/TiO_2-graphene, 1.0 La/TiO_2-graphene, and 1.5 La/TiO_2-graphene.

the result of increased absorbing and scattering of photon by surplus lanthanum in the photoreaction system. Based on the above results of visible-light photocatalytic activity tests of photocatalysts, we propose the probable synergistic effect mechanism between La/TiO_2 and graphene for the enhancement of photocatalytic activity. First, the incorporation of graphene having layered structure achieved a stronger adsorption of RhB on La/TiO_2-graphene photocatalyst. Due to the enhanced adsorption, the photoformed electrons that are produced during photocatalysis can readily migrate to doped La through graphene, and then easily reduce dioxygen, or other electron acceptor groups present in the liquid medium. As a result, electron–hole recombination is largely prevented, and this further favors the production of more OH radicals at the valance band of TiO and superoxide radical anion (O •−) at the La surface, which in turn results in faster degradation of RhB.[39] Sec-

ond, the graphene in the composite can act as effective electron transfer station, since it exhibits high electrical conductivity and high electron storage capacity, due to its two-dimensional-conjugation structure. Therefore, the graphene in the composite system served as an acceptor and transporter of the photogenerated electrons of TiO_2, and effectively suppressed the charge recombination, which is favorable for the improvement of photocatalytic activity.[40] Furthermore, the strong interaction and intimate contact between La/TiO_2 nanoparticles and graphene enhanced the transmission stability of photogenerated electron between the graphene and conduction band of TiO_2.[41] Finally, the cooperative effects of extended light absorption, charge separation, stabilization, and hindered charge recombination favored the enhancement of photocatalytic activity of the composite catalyst.

Preliminary photocatalytic reactions: The photocatalytic activity of the prepared and characterized graphene-La/TiO_2 material was assessed by the degradation of RhB under visible light irradiation in a slurry type photoreactor. Preliminary studies on the effect of the solution pH, catalyst amount, and initial dye concentration were carried out. The effect of the solution pH by varying the pH of the reaction solution between 2 and 12, and the effect of the aqueous pH on the degradation of RhB by the La/TiO_2-graphene catalyst was studied. *Fig.* 12(a) shows the results of employing a catalyst dosage of 1.5 g/L at each pH to treat 10 mg/L solutions of RhB. The pH of the various solutions was adjusted using 0.1N HCl and NaOH. After an irradiation period of 1 h, the catalyst showed high activity at all values of pH, with a maximum of 97.8% degradation at neutral pH.

Normally La can react with acids to produce its corresponding salt at low pH values while at alkaline pH, it reacts with a base to form complexes and neutral pH isideally suited for better performance.

Thus all further reactions were carried out at neutral pH. The effect of catalyst dosage, and the amount of catalyst required for efficient dye degradation were determined by carrying out the photodegradation reactions with different catalyst loadings from 0.5 to 2.5 g/L. Irradiation time (60 min) and pH 7 were kept constant. *Fig.* 12(b) clearly shows that until a dosage of 1.5 g/L, a linear relationship obtains between the percentage of dye degradation and catalyst dosage. Beyond this dosage, the graph reaches a plateau, wherein further increase in the amount of catalyst does not lead to significant increase in the extent of dye degradation. The increase of the catalyst amount could lead to increase the number of avai-lable adsorption and cat-

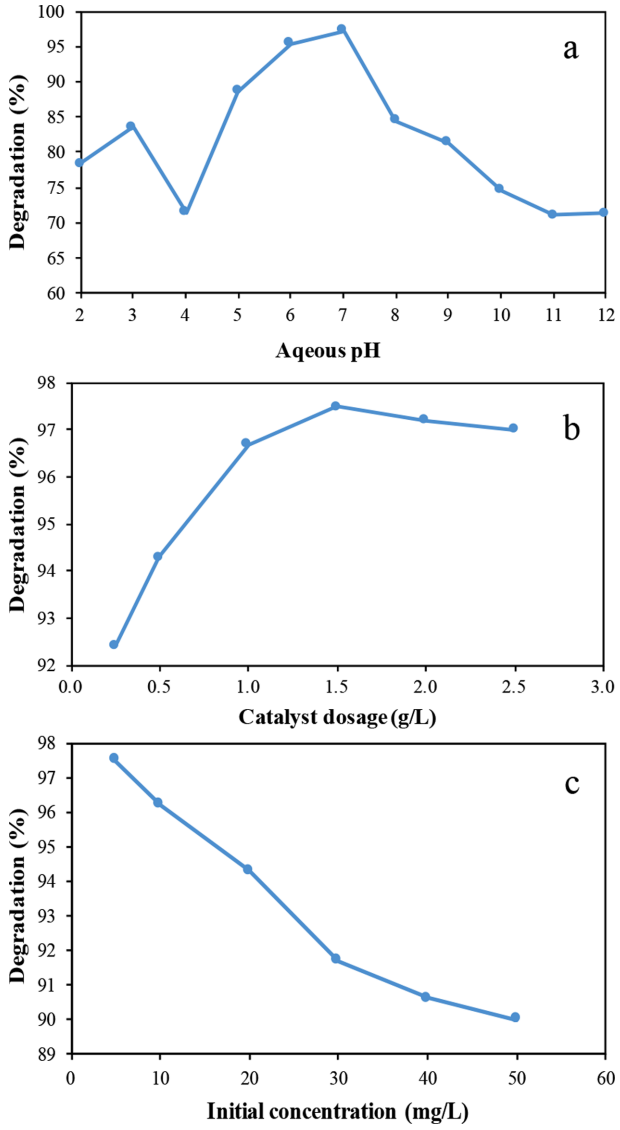

***Figure* 12.** (a) Effect of pH, (b) effect of catalyst dosage, and (c) effect of initial dye concentration.

alytic sites for the degradation of RhB. However, degradation efficiency remains almostthe same when the La/TiO_2-graphene dose was increased to 1.5 g/L. The reason may be attributed to the factthat increasing the La/TiO_2-graphene dose, the La concentration was also increased in the solution. The excess of La ions in the heterogeneous Fenton process could act as scavengers, which may hinder further improvement in degradation efficiency beyond 1 g/L.

This could be due to the decreased light penetration in solutions of high catalyst dosage. Thus, all further photodegradation studies were carried out with a catalyst dosage of 1.5 g/L. *Fig.* 12(c) shows the results obtained for the effect of initial dye concentration, which was studied by carrying out photodegradation reactions with a catalyst dosage

of 1.5 g/L for solutions of different dye concentrations under visible light irradiation for 1 h. When the initial RhB concentration was increased from 5 to 50 mg/L, the extent of dye degradation showed a slight decrease from 97.3 to 90.2%. The catalyst exhibited good efficiency, even for high initial dye concentrations. As the initial concentration increases, the degradation of dyes decreases This relates to the formation of HO^- radicals reacting with dye molecules. As the active sites are covered with the dye ions, generation of HO^- radicals on the surface of the catalyst is reduced and also the path length of the photons entering the dye solution decreases. Similar findings were reported by Rauf *et al.*[42] The results clearly demonstrated that the photocatalytic degradation process was efficient at low concentration of dyes.

Repetitive use of graphene-La/TiO_2 catalyst: *Fig.* 13 shows the recycle photocatalytic performance. After the first use, the performance reduces, but for the following cycles remains stable. In addition, the results demonstrate that after four cycles, the photoactivity of La/TiO_2-graphene decreased by 5.8%. It can be seen that graphene-La/TiO_2 showed relatively good stability. The slight decrease in photoactivity can be attributed to the residual dye absorbed in the composite film, which would reduce the photocatalytic performance of the film. The absorption basically reaches a equilibrium state after the first use and regeneration, thus subsequent recycling will not further affect the photocatalytic performance of the catalyst. Above all, this kind of photocatalyst can be directly separated from the solution, which could effectively reduce the cost of regeneration, and save a lot of time.

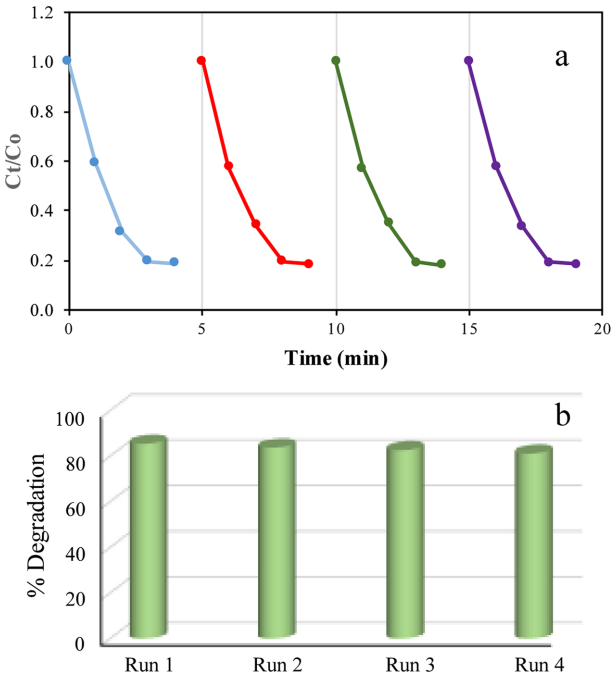

***Figure* 13.** (a) Cycling runs of the photo degradation. (b) Percent degradation of RhB with La/TiO_2-graphene.

Possible photocatalytic mechanism: *Fig.* 14 shows the possible photocatalytic mechanism of the La/TiO_2-graphene catalyst under UV and visible light irradiation that we propose on the basis of the above discussion. UV light excitation of TiO_2 generates electron-hole pairs (Eq. (1)). The photogenerated electrons move from the valence band (VB) to the conduction band (CB) of TiO_2, and are then transported to the GO nanosheets, facilitating oxygen reduction (Eq. (2)). Due to the difference in the work function of GO and the CB of anatase TiO_2, the delocalized electrons from the RhB reside in the aromatic structure of GO, suppressing their recombination with VB holes, which results in higher photocatalytic activity.

In addition to the inhibited recombination of holes and electrons, the GO nanosheets can mitigate the mass transfer constraint by increasing the availability of RhB near the TiO_2 surface.[43] The low energy state (positive redox potential) of photogenerated holes in the VB also helps to promote the RhB degradation by either direct oxidation of RhB, or

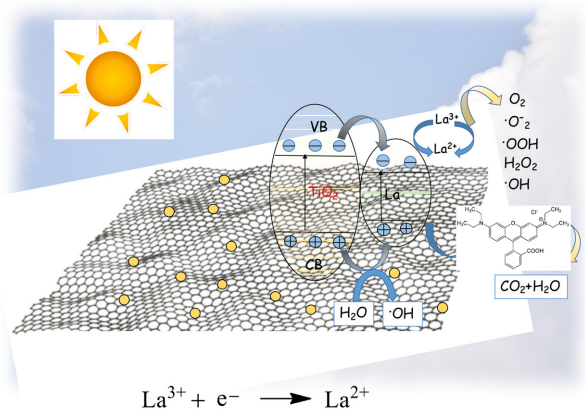

$$La^{3+} + e^- \longrightarrow La^{2+}$$
$$O_2 + e^- \longrightarrow O_2^{\bullet -}$$
$$O_2^{\bullet -} + La^{3+} \longrightarrow La^{2+}$$
$$La^{2+} + O_2 \longrightarrow La^{3+} + O_2^{\bullet -}$$
$$O_2^{\bullet -} + H \longrightarrow {}^{\bullet}OOH$$
$${}^{\bullet}OOH + H^+ + e^- \longrightarrow H_2O_2$$
$$h^+ + H_2O_2 \longrightarrow {}^{\bullet}O_2H + H^+$$
$$H_2O_2 + e^- \longrightarrow {}^{\bullet}OH + OH^{\bullet -}$$
$$h^+ + OH^- \longrightarrow {}^{\bullet}OH$$
$${}^{\bullet}OH + \text{dye} \longrightarrow \text{degradation product}$$

***Figure* 14.** Possible mechanism of charge separation and photocatalytic process over La/TiO_2-graphene under visible-light irradiation.

by generating HO• radicals (Eqs. (3) and (4)) that later oxidize RhB (Eq. (5)).[44,45] Moreover, the possible mechanism involved in the photocatalytic degradation of La doped TiO_2 has been proposed as follows (*Fig*. 14). Under visible light irradiation, electrons are excited from valance band to the conduction band of TiO_2, and holes (h) are produced. La^{3+} dopant in TiO_2 can effectively scavenge e^-, and inhibit their recombination with h^+, due to the existence of a partially filled orbital. The produced La^{2+} ions are very unstable, so that e^- can be easily descavenged, and passed to the adsorb O_2 molecules, subsequently promoting O_2^-• and OH• formation.[46] Simultaneously, the adsorbed photogenerated holes oxidize water molecules or surface bound hydroxide species to generate ·OH species.[47] *Fig.* 14 shows the degradation mechanism for La doped TiO_2. Thus the scavenging and transferring of the charge carrier within the TiO_2 surface may be attributed to La^{3+} dopant within the crystal structure that further improves the photocatalytic activity of the catalyst.

In addition to the inhibited recombination of holes and electrons, the GO nanosheets can mitigate the mass transfer constraint by increasing the availability of RhB near the TiO_2 surface.[43] The low energy state (positive redox potential) of photogenerated holes in the VB also helps to promote the RhB degradation by either direct oxidation of RhB, or by generating HO• radicals (Eqs. (3) and (4)) that later oxidize RhB (Eq. (5)).[44,45] Moreover, the possible mechanism involved in the photocatalytic degradation of La doped TiO_2 has been proposed as follows (*Fig*. 14). Under visible light irradiation, electrons are excited from valance band to the conduction band of TiO_2, and holes (h) are produced. La^{3+} dopant in TiO_2 can effectively scavenge e^-, and inhibit their recombination with h^+, due to the existence of a partially filled orbital. The produced La^{2+} ions are very unstable, so that e^- can be easily descavenged, and passed to the adsorb O_2 molecules, subsequently promoting O_2^-• and OH• formation.[46] Simultaneously, the adsorbed photogenerated holes oxidize water molecules or surface bound hydroxide species to generate ·OH species.[47] *Fig.* 14 shows the degradation mechanism for La doped TiO_2. Thus the scavenging and transferring of the charge carrier within the TiO_2 surface may be attributed to La^{3+} dopant within the crystal structure that further improves the photocatalytic activity of the catalyst.

CONCLUSION

La/TiO_2-graphene composite photocatalytic were prepared by a two-step hydrothermal method. Compared with pure TiO_2, the prepared composite catalysts showed enhanced photocatalytic activity under visible-light irradiation for RhB degradation. The higher photocatalytic activity of the composite catalyst could be attributed to extended light absorption, efficient charge separation, and enhanced adsorptivity on the composite catalyst surface, due to the two-dimensional planar structure of graphene, and the possibility of more interaction between composite and organic compound. The La/TiO_2-graphene composites described here will provide further benefits in future graphene-based research and technologies.

REFERENCES

1. Robinson, T.; McMullan, G.; Marchant, R.; Nigam, P. *Bioresour. Technol.* **2001**, *77*, 247.
2. Kobylewski, S.; Jacobson, M. F. Food Dyes: A Rainbow of Risks; Center for Science in The Public Interest: Washington, DC, 2010.
3. OECD, Emission Scenario Document on Textile Finishing Industry Europe, OECD, Paris, 2004, 77.
4. Leary, R.; Westwood, A. *Carbon*. **2011**, *49*, 741.
5. Lavanyaa, T.; Duttab, M.; Ramaprabhua, S.; Satheeshc, K. *J. Environ. Chem. Eng*. **2017**, *5*, 494.
6. Yadav, H. M.; Kim, J. S. *J. Alloys Compd*. **2016**, *688*, 123.
7. Meng, F.; Hong, Z.; Arndt, J., Li, M.; Zhi, Mi.; Yang, F.; Wu, N. *Nano Res*. **2012**, *5*, 213.
8. Wang, J.; Tafen, D. N., Lewis, J.P.; Hong, Z.; Manivannan A.; Zhi, M.; Li, M.; Wu, N. *J. Am. Chem. Soc*. **2009**, *131*, 12290.
9. Minella, M.; Sordello F.; Minero, C. *Catal. Today*. **2017**, *281*, 29.
10. Liu, L.; Luo, C.; Xiong, J.; Yang, Z.; Zhang, Y.; Cai, Y.; Gu, H. *J. Alloys Compd*, **2017**, *690*, 771.
11. Ilyas, A. M.; Gondal, M. A.; Baig, Umair.; Akhtar, S.; Yamani, Z. H. *Sol. Energy.* **2016**, *137*, 246.
12. Zargari, S.; Rahimi, R.; Ghaffarinejad, A.; Morsali, A. *J. Colloid Interface Sci.* **2016**, *466*, 310.
13. Yang, Y.; Li, Y.; Wang, J.; Wu, J.; He, D.; Qier, A. *J. Alloys Compd*. **2017**, *699*, 47.
14. Laia, C.; Wanga, M. M.; Zenga, G. M.; Liua, Y. G. *Appl. Surf. Sci*. **2016**, *390*, 368.
15. Wang, M.; Cai, L.; Jin, Q. *Sep. Purif. Technol*. **2017**, *172*, 217.
16. Ghasemia, S.; Hashemian, S. J.; Alamolhoda, A. A.; Gocheva, I.; Setayesh, S. R. *Mater. Res. Bull*. **2017**, *87*, 40.
17. Bera, S.; Pal, M.; Naskar, A.; Jana, S. *J. Alloys Compd.* **2016**, *669*, 177.
18. Tan L. L.; Ong, W. J., Chai, S. P.; Mohamed, A. R. *Chem. Eng. J*. **2017**, *308*, 248.
19. Sima, L. C., Leong, K. H.; Saravanan, P.; Ibrahim, S. *Appl. Surf. Sci*. **2016**, *358*, 122.
20. Lin, L.; Wang, H.; Xu, P. *Chem. Eng. J*. **2017**, *310*, 389.

21. Cao, S.; Liu, T.; Tsang, Y.; Chena, C. *Appl. Surf. Sci*. **2016**, *382*, 225.
22. Saleem, H.; Habib, J. *Alloys Compd.* **2016**, *679*, 177.
23. Qin, L.; Liang, S.; Tan, X.; Pan, A. *J. Alloys Compd.* **2017**, *692*, 124.
24. Raza, W.; Haque, M. M.; Muneer, M.; Fleisch, M.; Hakki, A.; Bahnemann, D. *J. Alloys Compd.* **2015**, *632*, 837.
25. Luan, X.; Chen, L.; Zhang, J.; Qu, G.; Flake, J. C.; Wang, Y. *Electrochim. Acta*. **2013**, *111*, 216.
26. Zhang, J. J.; Liu, X.; Ye, T.; Zheng, G. P.; Zheng, X.; Liu, P.; Guan, X. X. *J. Alloys Compd.* **2017**, *698*, 819.
27. Xie, Y.; Song, J.; Zhou, P.; Ling, Y.; Wu, Y. *Electrochim. Acta.* **2016**, *210*, 358.
28. Zhang, Y.; Hou, X.; Sun, T.; Zhao, X. *Ceram. Int*. **2017**, *43*, 1150.
29. Xu, W.; Xie, W.; Huang, X.; Chen, X.; Huang, N.; Wang, X.; Liu, J. *Food Chem.* **2017**, *221*, 267.
30. Khannam, M.; Boruah, R.; Doluia S. K. *J. Photochem. Photobiol. A Chemistry*. **2017**, *335*, 248.
31. Yan, W. Y.; Zhou, Q.; Chena, X.; Yang, Y.; Zhang, Y.; Huang, X. J.; Wu, Y. C. *J. Hazard. Mater*. **2016**, *314*, 41.
32. Yang, W. D.; Li, Y. R.; Lee, Y. C. *Appl. Surf. Sci*. **2016**, *380*, 249.
33. Kim, J. H.; Choi, W.; Jung, H. G.; Oh, S. H.; Chung, K. Y. *J. Alloys Compd.* **2017**, *690*, 390.
34. Li, X.; Zhao, Y.; Wang, X.; Wang, J.; Gaskov A. M.; Akbar, S. A. *Sens. Actuators B*. **2016**, *230*, 330.
35. Li, X.; Zhang, X.; Wang, R.; Su, Z.; Sha, J.; Liu, P. *J. Power Sources*. **2016**, *336*, 298.
36. Qu, A.; Xie, H.; Xu, Xi.; Zhang, Y.; Wen, S.; Cui, Y. *Appl. Surf. Sci*. **2016**, *375*, 230.
37. Zhang, J.; Liu, X.; Ye, T.; Zheng, G.; Zheng, X. C.; Liu, P.; Guan, X. X. *J. Alloys Compd*. **2017**, *698*, 819.
38. Chen, J.; Shu, J.; Anqi, Z.; Juyuan, H.; Yan, Z.; Chen, J. *Diamond Relat. Mater*. **2016**, *70*, 137.
39. Aparicio, J. R.; Samaniego, J. E.; Ramirez, B. R. *Sol. Energy*. **2016**, *139*, 258.
40. Biris, A. R.; Toloman, D.; Popa, A.; Lazar, M. D. *Physica E.* **2016**, *81*, 326.
41. Zhang, W.; Xiao, X.; Zeng, X.; Li, Y.; Zheng, L.; Wan, C. *J. Alloys Compd*. **2017**, *685*, 774.
42. Rauf, M. A.; Salman, S. *Chem. Eng. J*. **2009**, *151*, 10.
43. Prabhakarrao, N.; M. Chandra, R.; Rao, T. S. *J. Alloys Compd.* **2017**, *694*, 596.
44. Wang, W.; Yu, J.; Xiang, Q.; Bei, C. *Appl. Catal., B.* **2012**, *119*, 109.
45. Yang, L.; Li, Z.; Jiang, H.; Jiang, W.; Su, R.; Luo, S.; Luo Y. *Appl. Catal., B.* **2016**, **183**, 75.
46. Zhou, Y.; Wu, Y.; Li, Y.; Liu, Y.; Yang, L. *Ceram. Int.* **2016**, *42*, 12482.
47. Ghasemia, S.; Esfandiar, A.; Setayesh, S. R.; Yangjehc, A. H. A.; zad, I.; Gholamia, M. R. *Appl. Catal., A*. **2013**, *462*, 82.